remote sensing

MDPI

Technical Note

Integration of Surface Reflectance and Aerosol Retrieval Algorithms for Multi-Resolution Aerosol Optical Depth Retrievals over Urban Areas

Muhammad Bilal [1], Alaa Mhawish [1], Md. Arfan Ali [1], Janet E. Nichol [2], Gerrit de Leeuw [3,4,5], Khaled Mohamed Khedher [6,7], Usman Mazhar [8], Zhongfeng Qiu [1,*], Max P. Bleiweiss [9] and Majid Nazeer [10]

1 School of Marine Sciences, Nanjing University of Information Science and Technology, Nanjing 210044, China; muhammad.bilal@connect.polyu.hk (M.B.); alaa.mhawish@bhu.ac.in (A.M.); md.arfanali@nuist.edu.cn (M.A.A.)
2 Department of Geography, School of Global Studies, University of Sussex, Brighton BN1 9RH, UK; janet.nichol@connect.polyu.hk
3 Royal Netherlands Meteorological Institute (KNMI), R & D Satellite Observations, 3730 AE De Bilt, The Netherlands; gerrit.de.leeuw@knmi.nl
4 Aerospace Information Research Institute, Chinese Academy of Sciences (AirCAS), No. 20 Datun Road, Chaoyang District, Beijing 100101, China
5 School of Environment Science and Spatial Informatics, University of Mining and Technology, Xuzhou 221116, China
6 Department of Civil Engineering, College of Engineering, King Khalid University, Abha 61421, Saudi Arabia; kkhedher@kku.edu.sa
7 Department of Civil Engineering, High Institute of Technological Studies, Mrezgua University Campus, Nabeul 8000, Tunisia
8 School of Remote Sensing & Geomatics Engineering, Nanjing University of Information Science and Technology, Nanjing 210044, China; usman.mazhar@nuist.edu.cn
9 Department of Entomology, Plant Pathology and Weed Science, New Mexico State University, Las Cruces, NM 88003, USA; maxb@nmsu.edu
10 Key Laboratory of Digital Land and Resources, East China University of Technology, Nanchang 330013, China; majidnazeer@ecut.edu.cn
* Correspondence: zhongfeng.qiu@nuist.edu.cn

Abstract: The SEMARA approach, an integration of the Simplified and Robust Surface Reflectance Estimation (SREM) and Simplified Aerosol Retrieval Algorithm (SARA) methods, was used to retrieve aerosol optical depth (AOD) at 550 nm from a Landsat 8 Operational Land Imager (OLI) at 30 m spatial resolution, a Terra-Moderate Resolution Imaging Spectroradiometer (MODIS) at 500 m resolution, and a Visible Infrared Imaging Radiometer Suite (VIIRS) at 750 m resolution over bright urban surfaces in Beijing. The SEMARA approach coupled (1) the SREM method that is used to estimate the surface reflectance, which does not require information about water vapor, ozone, and aerosol, and (2) the SARA algorithm, which uses the surface reflectance estimated by SREM and AOD measurements obtained from the Aerosol Robotic NETwork (AERONET) site (or other high-quality AOD) as the input to estimate AOD without prior information on the aerosol optical and microphysical properties usually obtained from a look-up table constructed from long-term AERONET data. In the present study, AOD measurements were obtained from the Beijing AERONET site. The SEMARA AOD retrievals were validated against AOD measurements obtained from two other AERONET sites located at urban locations in Beijing, i.e., Beijing_RADI and Beijing_CAMS, over bright surfaces. The accuracy and uncertainties/errors in the AOD retrievals were assessed using Pearson's correlation coefficient (r), root mean squared error (RMSE), relative mean bias (RMB), and expected error (EE = $\pm$ 0.05 $\pm$ 20%). EE is the envelope encompassing both absolute and relative errors and contains 68% ($\pm 1\sigma$) of the good quality retrievals based on global validation. Here, the EE of the MODIS Dark Target algorithm at 3 km resolution is used to report the good quality SEMARA AOD retrievals. The validation results show that AOD from SEMARA correlates well with AERONET AOD measurements with high correlation coefficients (r) of 0.988, 0.980, and 0.981; small RMSE of 0.08, 0.09, and 0.08; and small RMB of 4.33%, 1.28%, and -0.54%. High percentages of retrievals, i.e.,

check for updates

Citation: Bilal, M.; Mhawish, A.; Ali, M.A.; Nichol, J.E.; Leeuw, G.d.; Khedher, K.M.; Mazhar, U.; Qiu, Z.; Bleiweiss, M.P.; Nazeer, M. Integration of Surface Reflectance and Aerosol Retrieval Algorithms for Multi-Resolution Aerosol Optical Depth Retrievals over Urban Areas. *Remote Sens.* **2022**, *14*, 373. https://doi.org/10.3390/rs14020373

Academic Editor: Dimitrios Balis

Received: 20 December 2021
Accepted: 11 January 2022
Published: 13 January 2022

Publisher's Note: MDPI stays neutral with regard to jurisdictional claims in published maps and institutional affiliations.

85.71%, 91.53%, and 90.16%, were within the EE for Landsat 8 OLI, MODIS, and VIIRS, respectively. The results suggest that the SEMARA approach is capable of retrieving AOD over urban areas with high accuracy and small errors using high to medium spatial resolution satellite remote sensing data. This approach can be used for aerosol monitoring over bright urban surfaces such as in Beijing, which is frequently affected by severe dust storms and haze pollution, to evaluate their effects on public health.

Keywords: AOD; SARA; SREM; AERONET; MODIS; VIIRS; Landsat 8; Beijing

1. Introduction

Aerosol optical depth (AOD) is retrieved from satellite observations using a variety of methods depending, among others, on the sensor characteristics and the retrieval approach chosen [1,2]. Satellite-retrieved AOD is used by a wide scientific community to monitor and investigate atmospheric aerosol properties at regional to global scales. AOD enables understanding of how aerosols affect the Earth's climate system [3], atmospheric visibility [4], and public health [5]. Ground-based Sunphotometer networks, such as the AErosol RObotic NETwork (AERONET) [6], have been established worldwide for continuous measurements of aerosol optical properties, including AOD, with high temporal resolution. However, these point measurements have sparse coverage. This spatial limitation is overcome by satellite remote sensing, which provides near-real-time AOD information at a global scale. Satellite remote sensing provides operational AOD products at spatial resolutions of 1 km, 3 km, 4.4 km, 6 km, and 10 km from several sensors including Moderate Resolution Imaging Spectroradiometer (MODIS), Multi-angle Imaging Spectroradiometer (MISR), Visible Infrared Imaging Radiometer Suite (VIIRS), etc., [7–16]. AOD inversion is mainly sensitive to an accurate cloud mask, an appropriate selection of the aerosol model, an accurate estimation of the surface reflectance, or an effective decoupling of the surface and atmospheric contributions to the reflectance at the top-of-atmosphere (TOA) [1,17,18]. Similarly, an accurate surface reflectance estimation based on a Radiative Transfer Model (RTM) depends on precise and accurate AOD retrievals. In other words, the retrieval of either AOD or surface reflectance requires accurate knowledge of the effects of the other parameters on the measured TOA reflectance, and thus, retrieval algorithms for these variables depend on each other.

In the present study, surface reflectance was estimated using the SREM (Simplified and Robust Surface Reflectance Estimation Method) atmospheric correction method [19,20]. SREM is the simplest atmospheric correction method compared to other existing image-based and physical atmospheric correction methods. It performs surface reflectance inversion for VIS-SWIR bands based on the Satellite Signal in the Solar Spectrum-Vector (6SV) [21–23] RTM equations 'without' incorporating information on AOD, aerosol model, water vapor concentrations, ozone concentrations, and atmospheric gases. It only requires TOA reflectance/radiance and solar-sensor geometries to estimate surface reflectance. Previous studies [19,20] showed that the SREM estimated surface reflectance is similar to the surface reflectance obtained from operational surface reflectance products of Landsat 8 OLI (Operational Land Imager), MODIS (Moderate Resolution Imaging Spectroradiometer), and VIIRS (Visible Infrared Imaging Radiometer Suite). It should be noted that the SREM estimated surface reflectance is different from the Rayleigh-corrected TOA reflectance, which is only a subtraction of the Rayleigh reflectance from the TOA reflectance and does not incorporate total transmission and the atmospheric backscattering ratio. Details of the SREM atmospheric correction method can be found in Bilal et al. [19].

Monitoring of atmospheric aerosol properties over complex and mixed bright urban surfaces, such as in Beijing, is challenging, especially during high aerosol loading. The Simplified high-resolution Aerosol Retrieval Algorithm (SARA) has been developed using MODIS data with a spatial resolution of 500 m to retrieve AOD at a regional scale. SARA

does not create a comprehensive look-up table (LUT) for AOD inversion and can retrieve AOD directly for the green channel. SARA requires TOA reflectance/radiance, solar-sensor zenith and azimuth angles, and aerosol information to perform aerosol inversion by iterating a wide range of aerosol types (ω_0 = 0.30–1.0 and g = 0.0–1.0), as SARA does not have prior information of aerosol types over the region. Aerosol information can be obtained from the local AERONET site or any reliable remote sensing aerosol product. SARA results have been validated over the complex and bright urban surfaces in Hong Kong [24], over the mixed urban surfaces in Beijing during dust storms [25] and haze episodes [26], and over water surfaces [11]. The SARA retrieved AOD has also been used for the estimation of concentrations of fine particulate matter ($PM_{2.5}$) at 500 m resolution over Hong Kong and the Pearl River Delta (PRD) [27]. The SARA results are very promising compared to the previously published high-resolution aerosol retrieval algorithms [28–30].

The objective of this study is to introduce a new regional approach 'SEMARA', i.e., an integration of the SREM and SARA methods, which can accurately retrieve regional AOD over bright urban surfaces, such as Beijing, from multi-resolution remote sensing data. In previous studies of SARA AOD, surface reflectance was obtained from the operational surface reflectance products. For example, in the case of MODIS and Landsat 8 OLI, surface reflectance was obtained from MOD09 [24,25] and LaSRC [31] surface reflectance products, respectively. These operational products show positive and negative biases in surface reflectance over bright urban and hilly terrain surfaces, respectively, compared to the surface reflectance estimated by [19,20]. Therefore, the SEMARA integrated approach is expected to be an improvement as it obtains corrected surface reflectance from the SREM compared to MOD09 and LaSRC.

2. Dataset

2.1. Satellite Data

Remote sensing images from three satellite sensors, including Landsat 8 OLI, MODIS, and VIIRS, were obtained to retrieve AOD using the SEMARA approach described in Section 3. The Landsat 8 OLI Level-1 cloud-free TOA reflectance images and solar-sensor images at 30 m resolution were obtained on demand from the EROS Science Processing Architecture on Demand Interface (https://espa.cr.usgs.gov/; accessed on 14 August 2021) from 2013 to 2021. The MODIS Level-1b calibrated radiance product (MOD02HKM) at 500 m and geolocation product (MOD03) at 1000 m resolution for the year 2017 were downloaded from the Level-1 and Atmosphere Archive & Distribution System Distributed Active Archive Center (LAADS DAAC: https://ladsweb.modaps.eosdis.nasa.gov/; accessed on 14 August 2021). VIIRS Sensor Data Record (VIIRS_SDR) and SDR terrain corrected geolocation (GMTCO) products at 750 m resolution for the year 2017 were obtained from the NOAA Comprehensive Large Array-data Stewardship System (CLASS: https://www.avl.class.noaa.gov/; accessed on 14 August 2021). Terra and Aqua MODIS NDVI (Normalized Difference Vegetation Index) products from 2013 to 2021 were also obtained to evaluate the performance of the SEMARA approach for different land surfaces.

2.2. AERONET Data

AERONET Version 3 (V3) Level 1.5 (L1.5) AOD measurements [32] were obtained for the Beijing_RADI site from 2013 to 2021. V3 L2.0 AOD data at the Beijing site from 2013 to 2017 and V3 L1.5 AOD data at the Beijing_CAMS site from 2017 to 2021 were obtained from the AERONET website (https://aeronet.gsfc.nasa.gov/; accessed on 14 August 2021) (Table 1). In our previous study [26], we found a Pearson's correlation coefficient (r) = 1, slope = 1, and intercept = 0 between L1.5 and L2.0 AOD measurements. Therefore, L1.5 AOD was used when L2.0 AOD data were not available. AOD measurements from the Beijing site were used as an input in the SEMARA approach as explained in the research methodology section (Section 3). AOD data from the Beijing_RADI and Beijing_CAMS sites were used to validate the SEMARA retrieved AOD.

Table 1. AERONET AOD measurements were used in the present study.

AERONET Site	Longitude	Latitude	Altitude (m)	Time Period	
				Level 2.0	Level 1.5
Beijing	116.381°	39.977°	92	2013–2017	2018–2021
Beijing_CAMS	116.317°	39.933°	106	2013–2017	2018–2021
Beijing_RADI	116.379°	40.005°	59	-	2013–2021

3. Research Methods

3.1. Description of the SEMARA Approach

In the present study, AOD was retrieved with spatial resolutions of 30 m, 500 m, and 750 m using data in the green channels of Landsat 8 OLI, Terra-MODIS, and SNPP-VIIRS by application of the SEMARA approach (Equation (1a,b)), an integration of the SREM (Equation (1a)) [19] and the SARA (Equation (1b)) [24] algorithms.

$$\rho_s = \frac{\rho_{TOA} - \rho_R}{(\rho_{TOA} - \rho_R)S_{atm0} + T_{s0}T_{v0}} \tag{1a}$$

$$\tau_a = \frac{4\mu_s\mu_v}{\omega_o P_a}\left[\rho_{TOA} - \rho_R - \frac{T_s T_v \rho_s}{1 - \rho_s S_{atm}}\right] \tag{1b}$$

where

ρ_{TOA} = the top-of-atmosphere (TOA) reflectance, which is a function of measured spectral radiance (L_{TOA}), solar zenith angle, earth-sun distance (d) in the astronomical unit, and mean solar exoatmospheric radiation (E_{SUN}).
ρ_R = Rayleigh reflectance in the absence of aerosols.
λ = wavelength.
T_s = atmospheric transmittance on the sun-surface path (downward).
T_{s0} = same as T_s but in an aerosol-free atmosphere.
T_v = atmospheric transmittance on the surface-sensor path (upward).
T_{v0} = same as T_v but in an aerosol-free atmosphere.
ρ_s = SREM estimated surface reflectance.
S_{atm} = atmospheric backscattering ratio to account for multiple reflections between the surface and atmosphere.
S_{atm} = same as S_{atm} but in an aerosol-free atmosphere.
μ_s = cosine of the solar zenith angle.
μ_v = cosine of the sensor zenith angle.
P_a = aerosol phase function.
ω_o = single scattering albedo.
τ_a = SARA AOD.

To solve Equation (1a) for SREM estimated surface reflectance (ρ_s), the atmospheric transmissions T_{so} Equation (2a) and T_{vo} (Equation (2b) [33,34], Rayleigh reflectance (ρ_R, Equation (3)) based on air mass (M, Equation (3a)) [35], Rayleigh optical depth (τ_R, Equation (3b)) [36], Rayleigh phase function (P_R, Equation (3c)) [35], scattering angle (Θ, Equation (3d)), and atmospheric backscattering ratio (S_{atm}, Equation (4)) [19] were calculated for an aerosol-free atmosphere.

$$T_{s0}(\lambda) = e^{(-\tau_R/\mu_s)} + e^{(-\tau_R/\mu_s)}\left\{e^{(0.52\tau_R/\mu_s)} - 1\right\} \tag{2a}$$

$$T_{v0}(\lambda) = e^{(-\tau_R/\mu_v)} + e^{(-\tau_R/\mu_v)}\left\{e^{(0.52\tau_R/\mu_v)} - 1\right\} \tag{2b}$$

$$\rho_R(\lambda, \theta_s, \theta_v, \varphi) = P_R(\theta_s, \theta_v, \varphi)\,\frac{\left(1 - e^{-M\tau_R}\right)}{4\,(\mu_s + \mu_v)} \tag{3}$$

$$\tau_R(\lambda) = 0.008569(\lambda)^{-4}\left(1 + 0.0113\,(\lambda)^{-2} + 0.00013\,(\lambda)^{-4}\right) \tag{3a}$$

$$M(\theta_s, \theta_v) = \frac{1}{\mu_s} + \frac{1}{\mu_v} \tag{3b}$$

$$P_R(\Theta) = \frac{3A}{4}\left(1 + cos^2\Theta\right) + B\,;\, A = 0.9587256,\ B = 1 - A \tag{3c}$$

$$\Theta = cos^{-1}(cos\theta_s cos\theta_v + sin\theta_s sin\theta_v cos\phi) \tag{3d}$$

where

λ = wavelength in μm
τ_R = Rayleigh optical depth
θ_s = solar zenith angle
θ_v = sensor zenith angle
φ = relative azimuth angle

A and B are coefficients that account for the molecular asymmetry.

$$S_{atm0}(\lambda) = (0.92\tau_R)e^{-\tau_R} \tag{4}$$

Using Equations (2a,b)–(4) in Equation (1a,b), the SREM surface reflectance (ρ_s) can be estimated. The SREM method is described in detail in Bilal et al. [19].

To solve Equation (1b) for SARA AOD (τ_a), the atmospheric transmission (Equations (5a–c)) [33,34], the aerosol scattering phase function (P_a , Equation (6)), and the atmospheric backscattering ratio (S_{atm}, Equation (7)) [24,25] were calculated but 'with' incorporating information on aerosol particles.

$$T_s(\lambda) = e^{(-(\tau_R+\tau_A)/\mu_s)} + e^{(-(\tau_R+\tau_A)/\mu_s)}\left\{e^{(0.52\tau_R+\beta\tau_A/\mu_s)} - 1\right\} \tag{5a}$$

$$T_v(\lambda) = e^{(-(\tau_R+\tau_A)/\mu_v)} + e^{(-(\tau_R+\tau_A)/\mu_v)}\left\{e^{(0.52\tau_R+\beta\tau_A/\mu_v)} - 1\right\} \tag{5b}$$

$$\beta = (1 + g)/2 \tag{5c}$$

where g is the asymmetry factor.

$$P_a = \frac{1 - g^2}{[1 + g^2 + 2gcos(\pi - \Theta)]^{3/2}} \tag{6}$$

$$S_{atm}(\lambda) = \{0.92\tau_R + (1 - g)\tau_A\}\, e^{-(\tau_R+\tau_A)} \tag{7}$$

In Equations (5a–c) and (7), τ_A (AOD, where A represents AERONET) is an unknown parameter that can be obtained from the AERONET Sunphotometer or other remote sensing aerosol products. In the present study, τ_A is obtained from the Beijing AERONET site, another urban site besides Beijing_RADI and Beijing_CAMS, to solve Equations (5a–c) and (7). In Equations (1a,b), (5a–c)–(7), ω_o and g are unknown. The ω_o and g are derived using AERONET AOD (τ_A), which is required on the right-hand side of Equation (1b) for the calculation of the total atmospheric transmittances (T_sT_v) and atmospheric backscattering ratio (S_{atm}). This is achieved by varying ω_o and g within the ranges of 0.30–1.0 and 0.0–1.0, respectively, until AOD (τ_a) on the left-hand side (τ_a) of Equation (1b) becomes equal to the input AERONET AOD (τ_A) on the right-hand side of Equation (1b). In this way, the values of ω_o and g are selected such that τ_a equals τ_A in Equation (1b) when the TOA reflectance (ρ_{TOA}) is measured over the Beijing AERONET site. The selected values of ω_o and g are used to retrieve the AOD over regions away from the AERONET site and these values are kept spatially constant for a particular image scene. The values ω_o and g do not necessarily accurately represent the actual optical properties of the aerosol, since they are influenced by the simplifications involved in the SARA approach. The SARA algorithm is described in detail in [24,26].

In summary, the SEMARA AOD (Equation (1a,b)) at 550 nm was retrieved for Landsat 8 OLI at 30 m resolution ($SEMARA_{Landsat}$), MODIS at 500 m resolution ($SEMARA_{MODIS}$),

and VIIRS at 750 m resolution ($SEMARA_{VIIRS}$) by integrating the SREM surface reflectance method (ρ_s, Equation (1a) based on the set of Equations (2a,b)–(4), and the SARA method (τ_a, Equation (1b)) based on the set of Equations (1a), (3), and (5a–c)–(7).

3.2. Methods Used for Statistical Analysis

AERONET Sunphotometers do not provide AOD data at 550 nm; therefore, AOD data were interpolated to 550 nm using the Ångström exponent determined from the AOD at 440 and 675 nm ($\alpha_{440–675}$) and the AOD at 500 nm. To increase the number of statistical samples and to consider the spatial variability imposed by atmospheric motion, AERONET AOD (at least two measurements must be available) was averaged within ± 60 min of the Landsat 8, MODIS, and VIIRS overpass times over Beijing. The $SEMARA_{Landsat}$, $SEMARA_{MODIS}$, and $SEMARA_{VIIRS}$ retrieved AOD were averaged over 3 × 3 pixels (at least 2 out of 9 pixels must be available) centered on the AERONET site. It should be noted that different spatial coverage is used with respect to the spatial resolution of the satellite data to investigate the effect of spatial coverage during data sampling on the aerosol retrieval algorithm. For example, spatial coverages used in data sampling for Landsat 8, MODIS, and VIIRS are 0.0081 km^2, 2.25 km^2, and 5.06 km^2, respectively. SEMARA AOD retrievals were validated against AERONET AOD measurements obtained at two sites (Beijing_RADI and Beijing_CAMS) located in Beijing, a city with mixed bright urban land surfaces where the AOD is greatly influenced by severe dust storms and haze episodes. The slope (Equation (8)) and intercept (Equation (9)) between the SEMARA AOD and AERONET AOD were calculated using the reduced major axis (RMA) method, which can simultaneously account for errors in both x and y variables [10,19,37]:

$$slope = \left(\frac{S_{XY}}{S_{XX}}\right)/|r| \tag{8}$$

where $|r|$ is the absolute value of the Pearson correlation coefficient (r), and S_{XY} and S_{XX} can be calculated using Equations (8a) and (8b), respectively.

$$S_{XY} = \sum_{i=1}^{n}\left(X_i - \overline{X}\right)\left(Y_i - \overline{Y}\right) \tag{8a}$$

$$S_{XX} = \sum_{i=1}^{n}\left(X_i - \overline{X}\right)^2 \tag{8b}$$

$$intercept = \overline{Y} - (slope)\overline{X} \tag{9}$$

where

$\overline{X}$ = mean of X (AERONET) variable, and

$\overline{Y}$ = mean of Y (SEMARA) variable.

The quality and errors of the SEMARA AOD retrievals are reported using the Expected Error (EE, Equation (10)), the root mean squared error (RMSE, Equation (11)), and the relative mean bias (RMB, Equation (12)). EE is the envelope encompassing both absolute and relative error and contains 68% (±1 σ) of the good quality retrievals based on global validation [9,38,39]. Here, the EE for the MODIS Dark Target algorithm at 3 km resolution [8,9,12,40–42] is used to report the good quality SEMARA AOD retrievals.

$$EE = \pm(0.05 + 0.20 \times AERONET_{AOD}) \tag{10}$$

The upper and lower EE boundaries are calculated using Equations (10a) and (10b), respectively.

$$Upper\ EE\ boundary = AERONET_{AOD} + |EE| \tag{10a}$$

$$Lower\ EE\ boundary = AERONET_{AOD} - |EE| \tag{10b}$$

The percentage of SEMARA AOD retrievals within (wEE%), above (aEE%), and below (bEE%) the EE boundaries are reported using Equations (10c), (10d), and (10e), respectively:

$$wEE\% = (AERONET_{AOD} - |EE| \leq SEMARA_{AOD} \leq AERONET_{AOD} + |EE|) \times 100 \quad (10c)$$

$$aEE\% = (SEMARA_{AOD} \geq AERONET_{AOD} + |EE|) \times 100 \quad (10d)$$

$$bEE\% = (SEMARA_{AOD} \leq AERONET_{AOD} - |EE|) \times 100 \quad (10e)$$

where $|EE|$ is the absolute value of EE (Equation (10)).

$$RMSE = \sqrt{\frac{1}{n}\sum_{i=1}^{n}\left(SEMARA_{(AOD)i} - AERONET_{(AOD)i}\right)^2} \quad (11)$$

$RMSE = 0$ represents the collocated points on the 1:1 (x = y) line, and $RMSE > 0$ represents the collocated points scattered away from the 1:1 line.

$$RMB = \left(\frac{\overline{SEMARA}_{AOD} - \overline{AERONET}_{AOD}}{\overline{SEMARA}_{AOD}}\right) \times 100 \quad (12)$$

where $RMB > 0.0$ and $RMB < 0.0$ represent over-and under-estimation of AOD retrievals, respectively.

The performance of the SEMARA AOD retrievals was also evaluated for different aerosol loadings (low: AOD < 0.2; moderate: 0.2 < AOD < 0.4; high: AOD > 0.4) as well as for different land cover types. Land surface types are classified into three classes using NDVI, i.e., bright surfaces (NDVI $\leq$ 0.2), sparse vegetation (0.2 < NDVI $\leq$ 0.4), and moderate vegetation (0.4 < NDVI $\leq$ 0.6).

4. Results and Discussion

4.1. Validation of SEMARA AOD Retrievals

Figure 1 shows scatterplots of the SEMARA-retrieved AOD at 30 m resolution from Landsat 8 OLI ($SEMARA_{Landsat}$ AOD, Figure 1a), at 500 m resolution from Terra-MODIS ($SEMARA_{MODIS}$ AOD, Figure 1b), and 750 m resolution from VIIRS ($SEMARA_{VIIRS}$ AOD, Figure 1c) against AERONET AOD measurements at two AERONET sites (Beijing_CAMS and Beijing_RADI) located in Beijing, in an area with mixed and bright urban surfaces. In Figure 1, the solid and dotted black lines represent the 1:1 (y = x) and EE lines, respectively, and the solid red line represents the regression line calculated using the RMA regression (Equations (9) and (10)). In total, 126, 248, and 244 collocated AOD data pairs were available for Landsat-AERONET, MODIS-AERONET, and VIIRS-AERONET, respectively. The results show that $SEMARA_{Landsat}$, $SEMARA_{MODIS}$, and $SEMARA_{VIIRS}$ AOD retrievals are well-correlated with AERONET AOD measurements over the urban surfaces of Beijing as indicated by the high values of the Pearson's correlation coefficients, i.e., r = 0.988, 0.980, 0.981, and the slopes of 0.99, 1.01, and 1.0, respectively. For all satellite data, with different spatial resolutions, the collocated points were scattered around the 1:1 line as also indicated by the small values of RMSE = 0.08 for $SEMARA_{Landsat}$, 0.09 for $SEMARA_{MODIS}$, and 0.08 for $SEMARA_{VIIRS}$. A direct relationship was observed between the spatial resolution/coverage of the AOD retrieval and the RMB, i.e., the finer the spatial resolution, the higher the RMB value. For example, a higher RMB of 4.33% was observed for $SEMARA_{Landsat}$ AOD (spatial sampling window: $3 \times 3 = 0.0081$ km^2) and a lower RMB value (-0.54%) was observed for $SEMARA_{VIIRS}$ AOD (spatial sampling window: $3 \times 3 = 5.06$ km^2). This suggests that the resolution of the satellite sensor plays an important role in aerosol inversion. The overestimation of 4.33% in the $SEMARA_{Landsat}$ AOD retrievals may be attributable to a slight underestimation in the SREM estimated surface reflectance during moderate to low aerosol loadings (AOD < 0.25), compared to very high aerosol loading (AOD > 0.50). This overestimation also resulted in a somewhat higher percentage of $SEMARA_{Landsat}$-retrieved AOD above the EE, i.e., aEE% = 14.29, than for the AOD

retrieved using $SEMARA_{MODIS}$ (aEE% = 6.86), and $SEMARA_{VIIRS}$ (aEE% = 6.97). Overall, the SEMARA approach performance over the urban surfaces of Beijing was robust as indicated by the large percentage of good quality AOD retrievals within the EE, i.e., wEE% = 85.71, 91.53, and 90.16 for $SEMARA_{Landsat}$, $SEMARA_{MODIS}$, and $SEMARA_{VIIRS}$, respectively. Figure 1d shows the combined validation of the $SEMARA_{Landsat}$, $SEMARA_{MODIS}$, and $SEMARA_{VIIRS}$ AOD retrievals. Overall, the retrieved AOD, with different spatial resolution, was well-correlated with AERONET AOD with r = 0.982, slope = 1.01, intercept = 0.003, RMSE = 0.086, RMB = 1.31%, and 89.81% of the retrievals were within the EE (wEE%). SEMARA was tuned to the AERONET AOD at the Beijing site and the results showed the performance of SEMARA in an urban area with heavy traffic (the ring road and other major roads) and, thus, captured well the variety of aerosol concentrations. These results suggest that high-resolution AOD for multi-resolution satellite remote sensing data can be obtained by application of SEMARA over an urban surface with varying and relatively bright surfaces.

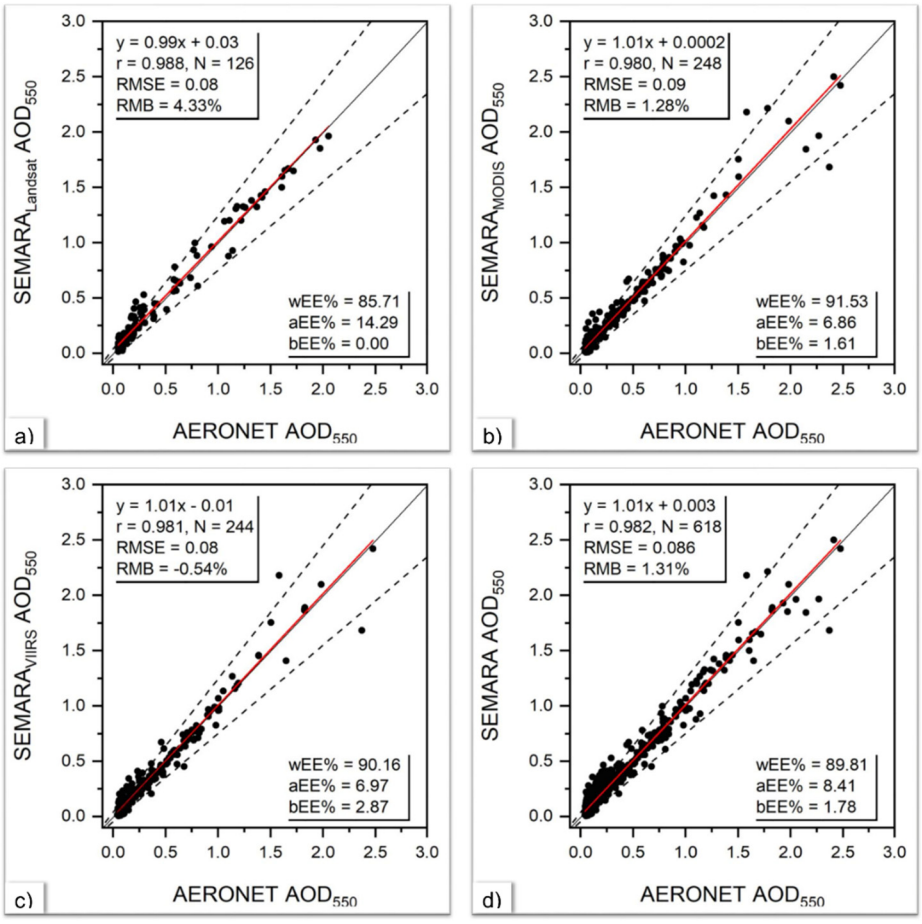

Figure 1. Validation of the SEMARA-retrieved AOD at (**a**) 30 m resolution from Landsat 8 OLI, (**b**) 500 m resolution from Terra-MODIS, (**c**) 750 m resolution from VIIRS, and (**d**) combined AOD retrievals from all three sensors, using AOD measured at two AERONET sites (Beijing_CAMS and Beijing_RADI) located in Beijing as independent references. The solid and dotted black lines represent the 1:1 (y = x) and EE lines, respectively, and the solid red line represents the regression line calculated using the RMA regression. Statistics metrics are provided in the legend in the top left corner of each figure.

4.2. SEMARA Performance for Different Aerosol Loadings

Several studies have shown that the accuracy of the retrieved AOD is affected by the aerosol loading in the atmospheric column [10,13,17,18,26,43]. In this section, we examine the performance of SEMARA retrievals for different aerosol loading (low: AOD $\leq$ 0.2;

moderate: 0.2 < AOD ≤ 0.4; high: AOD > 0.4). At low aerosol loading, uncertainties related to the surface reflectance estimation have a large influence on the AOD retrieval due to the relatively large contribution of the surface reflectance to the TOA reflectance. However, at high aerosol loading, aerosol contributes relatively more to the TOA reflectance, and the estimation of the microphysical properties of the aerosol particles greatly affects the AOD retrieval [18,44]. Table 2 shows that, for low aerosol loading, 88% of the combined SEMARA AOD retrievals for all sensors (Landsat 8, MODIS, and VIIRS) were within the EE with small RMSE (~0.05) and RMB (~2.50%). This indicates that in the SEMARA approach, the sensitivity of the AOD retrieval to the accurate estimation of the surface reflectance was effectively reduced by using an accurate AOD observation to estimate the aerosol parameters (ω_o and g Equation (1a,b)) used for AOD retrieval at other locations than the reference site. With increased aerosol loading and, thus, a relatively larger contribution of aerosol particles to the TOA reflectance, the performance of SEMARA was also good, with a large fraction of the AOD retrievals within the EE (wEE% = 88–94) and low RMSE (0.07–0.13). These results suggest that the SEMARA retrieval approach is capable of retrieving high AOD values without prior information about the aerosol microphysical properties.

Table 2. Performance of the SEMARA AOD retrievals during low, moderate, and high aerosol loading conditions. N represents the total number of collocations; aEE%, bEE%, and wEE% represent the percentage of retrievals above, below, and within the expected error; RMSE represents the root mean squared error and RMB represents relative mean bias.

AOD Level	N	aEE%	bEE%	wEE%	RMSE	RMB%
AOD ≤ 0.2	325	9.85	2.15	88.00	0.05	2.50
0.2 < AOD ≤ 0.4	110	10.91	0.91	88.18	0.07	4.96
AOD > 0.4	183	4.37	1.64	93.99	0.13	0.32

4.3. SEMARA Performance over Different Land Cover Types

The brightness of the land surface has a large influence on the AOD retrieval accuracy. The aerosol signal at the TOA over dark surfaces is relatively stronger than over bright surfaces [9,13,14,45–47]. Therefore, in this section, we examine the sensitivity of the SEMARA-retrieved AOD to the surface brightness, using the NDVI as a proxy, i.e., bright surfaces (NDVI < 0.2), sparse vegetation (0.2 < NDVI < 0.4), and moderate vegetation (0.4 < NDVI < 0.6). The greenness of the surface (NDVI) is larger over Beijing_RADI than over Beijing_CAMS, and the NDVI of Beijing_RADI varies seasonally with higher greenness during the spring and early summer. Figure 2 and Table 3 show that, for all three sensors, a larger number of collocated AOD retrievals was obtained for NDVI ≤ 0.2 than for 0.2 < NDVI ≤ 0.4 and for 0.4 < NDVI ≤ 0.6. The SEMARA approach for Landsat 8 performed better over bright surfaces and sparse vegetation than over moderate vegetation (Table 3). The relatively large error over moderate vegetation might be due to underestimation in SREM estimated surface reflectance, leading to overestimation in the SEMARA AOD retrievals, as indicated by aEE% ~ 25 and RMB ~ 13.35%. However, only 20 collocated Landsat-AERONET observations are available over these moderately vegetated surfaces. The SEMARA approach performed well for both MODIS and VIIRS for all three surface types with wEE% ~ 88.50–96.0 and 89.26–92.59, RMSE ~ 0.059–0.116 and 0.067–0.097, and RMB ~ −1.40–4.99% and −2.63–6.24, respectively.

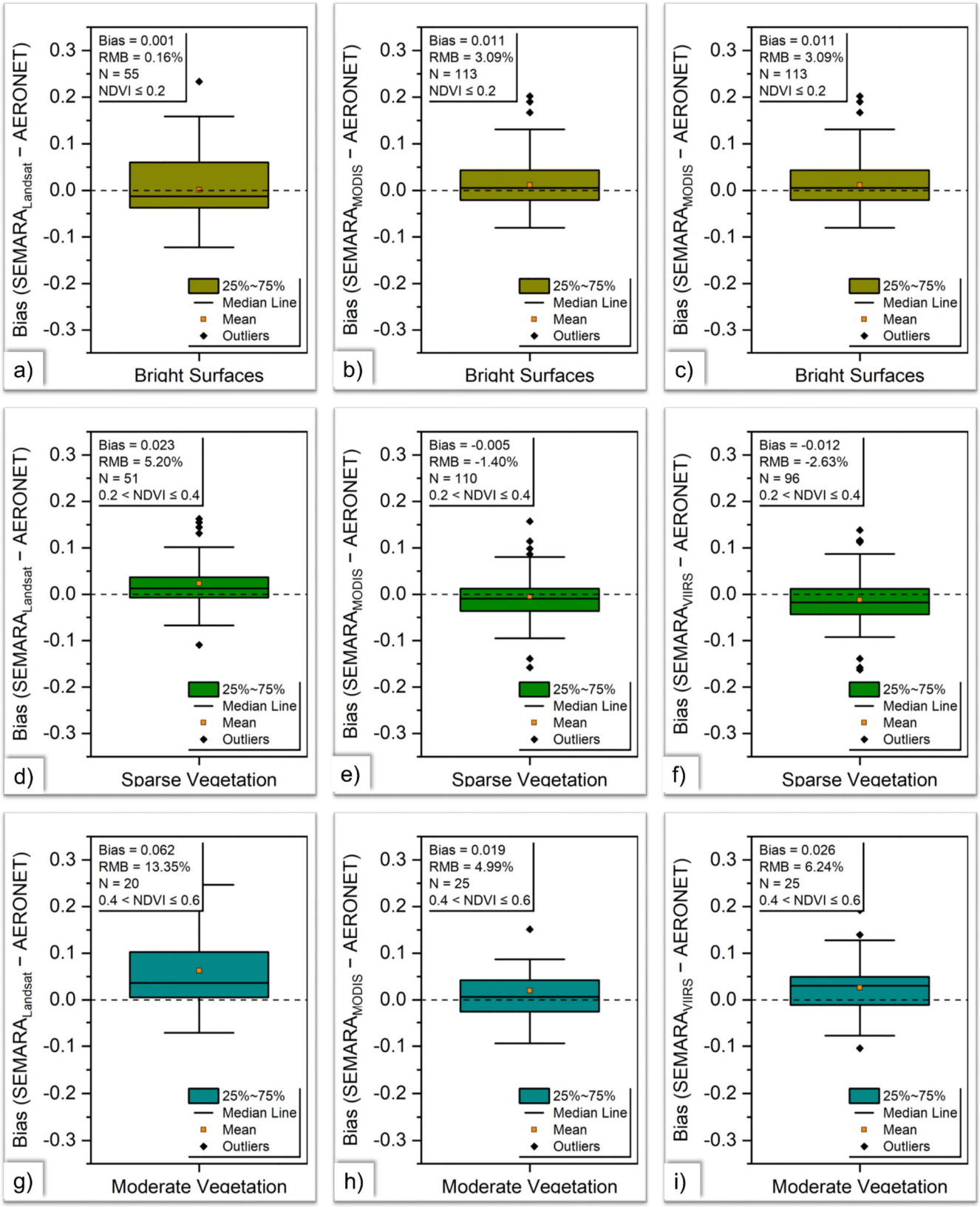

Figure 2. Box plots for bias (SEMARA AOD—AERONET AOD) over different land surfaces stratified based on NDVI values, i.e., (**a**–**c**) NDVI $\leq$ 0.2 (bright surfaces), (**d**–**f**) 0.2 < NDVI $\leq$ 0.4, and (**g**–**i**) 0.4 < NDVI $\leq$ 0.6.

Table 3. Performance of the $SEMARA_{Landsat}$, $SEMARA_{MODIS}$, and $SEMARA_{VIIRS}$ retrieved AOD over different land surface types, stratified according to NDVI values.

Land Cover Type	NDVI	Sensor	N	aEE%	bEE%	wEE%	RMSE	RMB%
Bright Surfaces	NDVI $\leq$ 0.2	Landsat 8	55	16.36	-	83.64	0.087	0.16
		MODIS	113	10.62	0.88	88.50	0.116	3.09
		VIIRS	121	8.26	2.48	89.26	0.097	−0.04
		All	289	10.73	1.38	87.89	0.100	1.27
Sparse Vegetation	0.2 < NDVI $\leq$ 0.4	Landsat 8	51	7.84	-	92.16	0.058	5.20
		MODIS	110	3.64	2.72	93.64	0.059	−1.40
		VIIRS	96	5.20	4.17	90.63	0.067	−2.63
		All	257	5.06	2.72	92.22	0.060	−0.54
Moderate Vegetation	0.4 < NDVI $\leq$ 0.6	Landsat 8	20	25.00	-	75.00	0.106	13.35
		MODIS	25	4.00	-	96.00	0.070	4.99
		VIIRS	27	7.41	-	92.59	0.067	6.24
		All	72	11.11	-	88.89	0.08	7.44

The overall performance of the combined SEMARA-retrieved AOD for all three sensors (Landsat 8, MODIS, and VIIRS) was good over all land surfaces, with 88–92% of the retrievals within the EE, small RMSE (~0.06–0.10), and RMB (−0.54–7.44%) (Table 3). These results suggest that the SEMARA approach is capable of retrieving AOD over different types of land surfaces. This study shows the robust performance of the SEMARA AOD retrieval approach over a highly polluted city (Beijing, China), which suggests that it can also be implemented in other geographical areas where a reference AOD value is available.

5. Conclusions

The SEMARA approach, based on the SREM and SARA methods, is introduced for the retrieval of AOD at 30 m resolution from Landsat 8 OLI, 500 m resolution from MODIS, and 750 m resolution from VIIRS. The SEMARA AOD retrievals were validated against the AOD measured at two AERONET sites with mixed and bright urban surfaces located in Beijing. The results show that the SEMARA-retrieved AOD is well-correlated with the AERONET AOD with high values of Pearson's correlation coefficient (r), low values of the RMSE and RMB, and a large percentage of retrievals within the EE (wEE%). A relatively large RMB value was observed for the $SEMARA_{Landsat}$ AOD when the surface was relatively dark (moderate vegetation), as compared to bright surfaces and sparse vegetation. This might be due to underestimation of the SREM estimated surface reflectance and this needs to be thoroughly investigated in future studies. Overall, the SEMARA approach performed well during different aerosol loading as well as over different land surfaces as characterized by the NDVI values. Therefore, the SEMARA approach is highly recommended for aerosol retrieval over mixed surfaces with low to high aerosol loading, using multi-resolution remote sensing data. SEMARA requires an accurate reference AOD value, which could be obtained from ground-based observations or satellite retrievals. The added value to satellite retrieved AOD values is the temporal extension both before and after the satellite overpass.

Author Contributions: Conceptualization, M.B.; methodology, M.B. and A.M.; software, M.B. and A.M.; validation, M.B. and A.M.; formal analysis, M.B. and A.M.; investigation, M.B. and A.M.; resources, M.B. and Z.Q.; data curation, M.B. and A.M.; writing—original draft preparation, M.B. and A.M.; writing—review and editing, M.B., A.M., M.A.A., J.E.N., G.d.L. and M.P.B.; visualization, M.B., A.M., M.A.A., K.M.K., U.M., M.P.B. and M.N.; supervision, M.B.; project administration, M.B. and Z.Q.; funding acquisition, M.B., Z.Q. and K.M.K. All authors have read and agreed to the published version of the manuscript.

Funding: This research was funded by the National Key Research and Development Program of China (2016YFC1400901), the Jiangsu Provincial Department of Education for the Special Project of Jiangsu Distinguished Professor (R2018T22), the Deanship of Scientific Research at King Khalid University (RGP.1/372/42), and the Startup Foundation for Introduction Talent of NUIST (2017r107).

Institutional Review Board Statement: Not applicable.

Informed Consent Statement: Not applicable.

Data Availability Statement: MODIS data is freely available at the Level-1 and Atmosphere Archive & Distribution System Distributed Active Archive Center (LAADS DAAC: https://ladsweb.modaps.eosdis.nasa.gov/, accessed on 14 August 2021), VIIRS data is freely available at the NOAA Comprehensive Large Array-data Stewardship System (CLASS: https://www.avl.class.noaa.gov/, accessed on 14 August 2021), and AERONET measurements are freely available at https://aeronet.gsfc.nasa.gov/, accessed on 14 August 2021).

Acknowledgments: The authors would like to acknowledge NASA's Level-1 and Atmosphere Archive and Distribution System (LAADS) Distributed Active Archive Center (DAAC) (https://ladsweb.modaps.eosdis.nasa.gov/; accessed on 14 August 2021) for MODIS data, the NOAA Comprehensive Large Array-data Stewardship System (CLASS: https://www.avl.class.noaa.gov/; accessed on 14 August 2021) for VIIRS data, and Principal Investigators of Beijing AERONET sites. The authors (Muhammad Bilal and Khaled Mohamed Khedher) extend their thanks to the Deanship of Scientific Research at King Khalid University for funding this work. We are thankful to Devin White (Oak Ridge National Laboratory) for MODIS Conversion Tool Kit (MCTK). The study contributes to the ESA/MOST cooperation project DRAGON5, Topic 3 Atmosphere, sub-topic 3.2 Air-Quality.

Conflicts of Interest: The authors declare no conflict of interest. The funders had no role in the design of the study; in the collection, analyses, or interpretation of data; in the writing of the manuscript, or in the decision to publish the results.

References

1. De Leeuw, G.; Holzer-Popp, T.; Bevan, S.; Davies, W.H.; Descloitres, J.; Grainger, R.G.; Griesfeller, J.; Heckel, A.; Kinne, S.; Klüser, L.; et al. Evaluation of seven European aerosol optical depth retrieval algorithms for climate analysis. *Remote Sens. Environ.* **2015**, *162*, 295–315. [CrossRef]
2. Kokhanovsky, A.A.; de Leeuw, G. *Satellite Aerosol Remote Sensing over Land*; Springer: Berlin/Heidelberg, Germany, 2009. [CrossRef]
3. Kaufman, Y.J.; Tanré, D.; Boucher, O. A satellite view of aerosols in the climate system. *Nature* **2002**, *419*, 215–223. [CrossRef] [PubMed]
4. Cheung, H.-C.; Wang, T.; Baumann, K.; Guo, H. Influence of regional pollution outflow on the concentrations of fine particulate matter and visibility in the coastal area of southern China. *Atmos. Environ.* **2005**, *39*, 6463–6474. [CrossRef]
5. Pope, C.A.; Ezzati, M.; Dockery, D.W. Fine-particulate air pollution and life expectancy in the United States. *N. Engl. J. Med.* **2009**, *360*, 376–386. [CrossRef] [PubMed]
6. Holben, B.N.; Eck, T.F.; Slutsker, I.; Tanré, D.; Buis, J.P.; Setzer, A.; Vermote, E.; Reagan, J.A.; Kaufman, Y.J.; Nakajima, T.; et al. AERONET—A Federated Instrument Network and Data Archive for Aerosol Characterization. *Remote Sens. Environ.* **1998**, *66*, 1–16. [CrossRef]
7. Levy, R.C.; Munchak, L.A.; Mattoo, S.; Patadia, F.; Remer, L.A.; Holz, R.E. Towards a long-term global aerosol optical depth record: Applying a consistent aerosol retrieval algorithm to MODIS and VIIRS-observed reflectance. *Atmos. Meas. Tech.* **2015**, *8*, 4083–4110. [CrossRef]
8. Remer, L.A.; Mattoo, S.; Levy, R.C.; Munchak, L.A. MODIS 3 km aerosol product: Algorithm and global perspective. *Atmos. Meas. Tech.* **2013**, *6*, 1829–1844. [CrossRef]
9. Levy, R.C.; Mattoo, S.; Munchak, L.A.; Remer, L.A.; Sayer, A.M.; Patadia, F.; Hsu, N.C. The Collection 6 MODIS aerosol products over land and ocean. *Atmos. Meas. Tech.* **2013**, *6*, 2989–3034. [CrossRef]
10. Bilal, M.; Mhawish, A.; Nichol, J.E.; Qiu, Z.; Nazeer, M.; Ali, M.A.; de Leeuw, G.; Levy, R.C.; Wang, Y.; Chen, Y.; et al. Air pollution scenario over Pakistan: Characterization and ranking of extremely polluted cities using long-term concentrations of aerosols and trace gases. *Remote Sens. Environ.* **2021**, *264*, 112617. [CrossRef]
11. Bilal, M.; Nazeer, M.; Nichol, J.E. Validation of MODIS and VIIRS derived aerosol optical depth over complex coastal waters. *Atmos. Res.* **2017**, *186*, 43–50. [CrossRef]
12. Nichol, J.; Bilal, M. Validation of MODIS 3 km Resolution Aerosol Optical Depth Retrievals Over Asia. *Remote Sens.* **2016**, *8*, 328. [CrossRef]

13. Sayer, A.M.; Munchak, L.A.; Hsu, N.C.; Levy, R.C.; Bettenhausen, C.; Jeong, M.J. MODIS Collection 6 aerosol products: Comparison between Aqua's e-Deep Blue, Dark Target, and "merged" data sets, and usage recommendations. *J. Geophys. Res. Atmos.* **2014**, *119*, 13965–13989. [CrossRef]
14. Hsu, N.C.; Jeong, M.-J.; Bettenhausen, C.; Sayer, A.M.; Hansell, R.; Seftor, C.S.; Huang, J.; Tsay, S.-C. Enhanced Deep Blue aerosol retrieval algorithm: The second generation. *J. Geophys. Res. Atmos.* **2013**, *118*, 9296–9315. [CrossRef]
15. Jackson, J.M.; Liu, H.; Laszlo, I.; Kondragunta, S.; Remer, L.A.; Huang, J.; Huang, H.-C. Suomi-NPP VIIRS aerosol algorithms and data products. *J. Geophys. Res. Atmos.* **2013**, *118*, 12673–12689. [CrossRef]
16. Witek, M.L.; Garay, M.J.; Diner, D.J.; Bull, M.A.; Seidel, F.C.; Nastan, A.M.; Hansen, E.G. Introducing the MISR level 2 near real-time aerosol product. *Atmos. Meas. Tech.* **2021**, *14*, 5577–5591. [CrossRef]
17. Mhawish, A.; Sorek-Hamer, M.; Chatfield, R.; Banerjee, T.; Bilal, M.; Kumar, M.; Sarangi, C.; Franklin, M.; Chau, K.; Garay, M.; et al. Aerosol characteristics from earth observation systems: A comprehensive investigation over South Asia (2000–2019). *Remote Sens. Environ.* **2021**, *259*, 112410. [CrossRef]
18. Mhawish, A.; Banerjee, T.; Sorek-Hamer, M.; Lyapustin, A.; Broday, D.M.; Chatfield, R. Comparison and evaluation of MODIS Multi-angle Implementation of Atmospheric Correction (MAIAC) aerosol product over South Asia. *Remote Sens. Environ.* **2019**, *224*, 12–28. [CrossRef]
19. Bilal, M.; Nazeer, M.; Nichol, J.E.; Bleiweiss, M.P.; Qiu, Z.; Jäkel, E.; Campbell, J.R.; Atique, L.; Huang, X.; Lolli, S. A Simplified and Robust Surface Reflectance Estimation Method (SREM) for Use over Diverse Land Surfaces Using Multi-Sensor Data. *Remote Sens.* **2019**, *11*, 1344. [CrossRef]
20. Nazeer, M.; Ilori, C.O.; Bilal, M.; Nichol, J.E.; Wu, W.; Qiu, Z.; Gayene, B.K. Evaluation of atmospheric correction methods for low to high resolutions satellite remote sensing data. *Atmos. Res.* **2021**, *249*, 105308. [CrossRef]
21. Vermote, E.F.; Kotchenova, S. Atmospheric correction for the monitoring of land surfaces. *J. Geophys. Res. Atmos.* **2008**, *113*, D23S90. [CrossRef]
22. Kotchenova, S.Y.; Vermote, E.F.; Levy, R.; Lyapustin, A. Radiative transfer codes for atmospheric correction and aerosol retrieval: Intercomparison study. *Appl. Opt.* **2008**, *47*, 2215. [CrossRef]
23. Kotchenova, S.Y.; Vermote, E.F.; Matarrese, R.; Frank, J.; Klemm, J. Validation of a vector version of the 6S radiative transfer code for atmospheric correction of satellite data. Part I: Path radiance. *Appl. Opt.* **2006**, *45*, 6762–6774. [CrossRef] [PubMed]
24. Bilal, M.; Nichol, J.E.; Bleiweiss, M.P.; Dubois, D. A Simplified high resolution MODIS Aerosol Retrieval Algorithm (SARA) for use over mixed surfaces. *Remote Sens. Environ.* **2013**, *136*, 135–145. [CrossRef]
25. Bilal, M.; Nichol, J.E.; Chan, P.W. Validation and accuracy assessment of a Simplified Aerosol Retrieval Algorithm (SARA) over Beijing under low and high aerosol loadings and dust storms. *Remote Sens. Environ.* **2014**, *153*, 50–60. [CrossRef]
26. Bilal, M.; Nichol, J.E. Evaluation of MODIS aerosol retrieval algorithms over the Beijing-Tianjin-Hebei region during low to very high pollution events. *J. Geophys. Res. Atmos.* **2015**, *120*, 7941–7957. [CrossRef]
27. Bilal, M.; Nichol, J.; Spak, S. A New Approach for Estimation of Fine Particulate Concentrations Using Satellite Aerosol Optical Depth and Binning of Meteorological Variables. *Aerosol Air Qual. Res.* **2017**, *11*, 356–367. [CrossRef]
28. Sun, L.; Wei, J.; Bilal, M.; Tian, X.; Jia, C.; Guo, Y.; Mi, X. Aerosol optical depth retrieval over bright areas using Landsat 8 OLI images. *Remote Sens.* **2016**, *8*, 23. [CrossRef]
29. Wong, M.S.; Nichol, J.E.; Lee, K.H. An operational MODIS aerosol retrieval algorithm at high spatial resolution, and its application over a complex urban region. *Atmos. Res.* **2011**, *99*, 579–589. [CrossRef]
30. Li, C.; Lau, A.K.-H.; Chu, D.A. Retrieval, validation, and application of the 1-km aerosol optical depth from MODIS measurements over Hong Kong. *IEEE Trans. Geosci. Remote Sens.* **2005**, *43*, 2650–2658. [CrossRef]
31. Bilal, M.; Qiu, Z. Aerosol Retrievals Over Bright Urban Surfaces Using Landsat 8 Images. In Proceedings of the IGARSS 2018–2018 IEEE International Geoscience and Remote Sensing Symposium, Valencia, Spain, 22–27 July 2018; pp. 7560–7563.
32. Holben, N.; Tanr, D.; Smirnov, A.; Eck, T.F.; Slutsker, I.; Newcomb, W.W.; Schafer, J.S.; Chatenet, B.; Lavenu, F.; Kaufman, J.; et al. An emerging ground-based aerosol climatology: Aerosol optical depth from AERONET. *J. Geophys. Res. Atmos.* **2001**, *106*, 12067–12097. [CrossRef]
33. Tanre, D.; Herman, M.; Deschamps, P.Y.; de Leffe, A. Atmospheric modeling for space measurements of ground reflectances, including bidirectional properties. *Appl. Opt.* **1979**, *18*, 3587–3594. [CrossRef] [PubMed]
34. Liu, C.-H.; Liu, G.-R. Aerosol Optical Depth Retrieval For Spot HRV Images. *J. Mar. Sci. Technol.* **2009**, *17*, 300–305. [CrossRef]
35. LISE. OLCI Level 2: Rayleigh Correction Over Land (S3-L2-SD-03-C15-LISE-ATBD). Available online: https://sentinels.copernicus.eu/documents/247904/349589/OLCI_L2_Rayleigh_Correction_Land.pdf (accessed on 17 October 2018).
36. Hansen, J.E.; Travis, L.D. Light scattering in planetary atmospheres. *Space Sci. Rev.* **1974**, *16*, 527–610. [CrossRef]
37. Harper, W.V. Reduced Major Axis Regression. In *Wiley StatsRef: Statistics Reference Online*; Wiley Online Library: Hoboken, NJ, USA, 2016. [CrossRef]
38. Remer, L.a.; Kaufman, Y.J.; Tanré, D.; Mattoo, S.; Chu, D.a.; Martins, J.V.; Li, R.-R.; Ichoku, C.; Levy, R.C.; Kleidman, R.G.; et al. The MODIS Aerosol Algorithm, Products, and Validation. *J. Atmos. Sci.* **2005**, *62*, 947–973. [CrossRef]
39. Sayer, A.M.; Govaerts, Y.; Kolmonen, P.; Lipponen, A.; Luffarelli, M.; Mielonen, T.; Patadia, F.; Popp, T.; Povey, A.C.; Stebel, K.; et al. A review and framework for the evaluation of pixel-level uncertainty estimates in satellite aerosol remote sensing. *Atmos. Meas. Tech.* **2020**, *13*, 373–404. [CrossRef]

40. Gupta, P.; Levy, R.C.; Mattoo, S.; Remer, L.A.; Munchak, L.A. A surface reflectance scheme for retrieving aerosol optical depth over urbansurfaces in MODIS Dark Target retrieval algorithm. *Atmos. Meas. Tech.* **2016**, *9*, 3293–3308. [CrossRef]
41. Munchak, L.A.; Levy, R.C.; Mattoo, S.; Remer, L.A.; Holben, B.N.; Schafer, J.S.; Hostetler, C.A.; Ferrare, R.A. MODIS 3 km aerosol product: Applications over land in an urban/suburban region. *Atmos. Meas. Tech.* **2013**, *6*, 1747–1759. [CrossRef]
42. Bilal, M.; Qiu, Z.; Campbell, J.R.; Spak, S.; Shen, X.; Nazeer, M. A New MODIS C6 Dark Target and Deep Blue Merged Aerosol Product on a 3 km Spatial Grid. *Remote Sens.* **2018**, *10*, 463. [CrossRef]
43. Bilal, M.; Nazeer, M.; Nichol, J.E.; Qiu, Z.; Wang, L.; Bleiweiss, M.P.; Shen, X.; Campbell, J.R.; Lolli, S. Evaluation of Terra-MODIS C6 and C6.1 Aerosol Products against Beijing, XiangHe, and Xinglong AERONET Sites in China during 2004–2014. *Remote Sens.* **2019**, *11*, 486. [CrossRef]
44. Bilal, M.; Qiu, Z.; Nichol, J.E.; Mhawish, A.; Ali, M.A.; Khedher, K.M.; de Leeuw, G.; Yu, W.; Tiwari, P.; Nazeer, M.; et al. Uncertainty in Aqua-MODIS Aerosol Retrieval Algorithms During COVID-19 Lockdown. *IEEE Geosci. Remote Sens. Lett.* **2021**, 1–5. [CrossRef]
45. Mhawish, A.; Banerjee, T.; Broday, D.M.; Misra, A.; Tripathi, S.N. Evaluation of MODIS Collection 6 aerosol retrieval algorithms over Indo-Gangetic Plain: Implications of aerosols types and mass loading. *Remote Sens. Environ.* **2017**, *201*, 297–313. [CrossRef]
46. Bilal, M.; Nazeer, M.; Qiu, Z.; Ding, X.; Wei, J. Global Validation of MODIS C6 and C6.1 Merged Aerosol Products over Diverse Vegetated Surfaces. *Remote Sens.* **2018**, *10*, 475. [CrossRef]
47. Bilal, M.; Nichol, J.; Wang, L. New customized methods for improvement of the MODIS C6 Dark Target and Deep Blue merged aerosol product. *Remote Sens. Environ.* **2017**, *197*, 115–124. [CrossRef]